Lehikoinen, Antti; Arkkio, Antero; Belahcen, Anouar

Reduced Basis Finite Element Modeling of Electrical Machines with Multiconductor Windings

Published in:
IEEE Transactions on Industry Applications

DOI:
10.1109/TIA.2017.2696509

Published: 01/01/2017

Document Version
Peer-reviewed accepted author manuscript, also known as Final accepted manuscript or Post-print

Please cite the original version:
Lehikoinen, A., Arkkio, A., & Belahcen, A. (2017). Reduced Basis Finite Element Modeling of Electrical Machines with Multiconductor Windings. *IEEE Transactions on Industry Applications*, *53*(5), 4252-4259. Article 7907188. https://doi.org/10.1109/TIA.2017.2696509

Reduced Basis Finite Element Modelling of Electrical Machines with Multi-Conductor Windings

Antti Lehikoinen, Antero Arkkio and Anouar Belahcen

***Abstract*—Finite element analysis of electrical machines with multi-conductor windings can be computationally costly. This paper proposes a solution to this problem, using a reduced basis approach. The field-circuit problem is first solved in a single slot only, with a set of different boundary conditions. These pre-computed solutions are then used as shape functions to approximate the solution in all slots of the full problem. A polynomial interpolation method is also proposed for coupling the slot domains with the rest of the geometry, even if the geometries or meshes do not fully conform on the boundary.**

The method is evaluated on several test problems both in the frequency- and time-domains. According to the simulations, accurate solutions are obtained, 54-90 times faster compared to the established finite element approach.

***Index Terms*—Finite element analysis, eddy currents, proximity effects, reduced order systems.**

I. Introduction

The prevailing efficiency and performance demands require an accurate prediction of resistive losses in the windings of an electrical machine. Outside very simple geometries, finite element (FE) analysis is typically required due to the eddy-current phenomena. However, this can be a computationally formidable task due to the dense mesh required, especially if the number of conductors is large. This is true especially at higher frequencies, e.g. when considering the effect of voltage harmonics from converter supply.

These high-frequency resistive losses can be divided into skin- and proximity-effect losses – the latter of which is typically dominant – and circulating currents. The former two are related to the uneven current density distribution *within a conductor*, whereas the latter refers to the uneven distribution of total current *between conductors* connected in parallel. Modelling both phenomena requires taking into account the conductor-level field solution as well as the total winding configuration.

The research leading to these results has received funding from the European Research Council under the European Unions Seventh Framework Programme (FP7/2007-2013) / ERC Grant Agreement n. 339380.

A. Lehikoinen, A. Arkkio and A. Belahcen are with Aalto University, Dept. of Electrical Engineering and Automation, P.O. Box 13000, FI-00076 Espoo, Finland. (e-mail: antti.lehikoinen@aalto.fi, antero.arkkio@aalto.fi, anouar.belahcen@aalto.fi).

A. Belahcen is also with Tallinn University of Technology, 19086 Tallinn, Estonia.

Color versions of one or more of the figures in this paper are available online at http://ieeexplore.ieee.org.

Proximity effects have been often analysed by time- or frequency-domain homogenization [1]–[8]. However, these studies have mostly focused on purely series-connected coils, or idealized Litz wires. By contrast, the scarce research on circulating currents has mostly ignored the proximity effects [9]–[12]. Some brute-force and analytical approaches have also been studied, typically with problems with relatively few conductors [13]–[23].

This paper proposes a reduced basis approach for analysing both the proximity and circulating current effects in a computationally efficient fashion, extending the work presented at the ICEM conference [24]. The method has been heavily inspired by the recently-proposed domain decomposition approach [25], but extends the analysis to the time-domain and addresses many of its drawbacks related to analysing electrical machines in particular. Indeed, the proposed method can be directly applied on arbitrary and uneven conductor packings inside a slot of any shape. Furthermore, a nonconforming coupling is proposed between the domains, allowing for easy handling of curved boundaries and a great liberty for meshing. Finally, the proposed method results in a significantly smaller problem in the online computation stage.

The accuracy and efficiency of the method are then evaluated on several demonstrative problems. The performance of the proposed coupling approach is first evaluated on a simplified problem. Then, nonlinear analysis is performed on a 500 kW induction machine both in the frequency- and time-domains. According to the simulations, the method is accurate and yields significant computational time savings in realistic problems. Thus, it could be very useful in the design and optimization of high-performance electrical machines.

II. Reduced Basis Approach

This paper proposes an approach for 2D field-circuit FE analysis of an electrical machine with a large number of conductors per stator slot. Using traditional techniques, this type of analysis would be computationally costly due to the large number of degrees-of-freedom (DoF) required for each slot. In the proposed method, a set of solutions is first computed for one slot and different boundary conditions. These solutions are then used as shape functions in the full problem, to approximate the solution in all slots of the machine. On the slot boundary, they are coupled together with the typical nodal-based shape functions. The method will be referred to as a reduced-basis approach due to the use of

pre-computed solutions. However, it obviously bears a close resemblance to domain decomposition methods as well.

Throughout this paper, the following terms are adopted. The slot domain with the pre-computed solutions is referred to as the *reduced domain*, whereas the rest of the machine excluding the slots is called *main domain*. Similar terminology is used for the meshes. The term *main problem* shall refer to analysing the full problem domain with the proposed method. The tilde notation $\tilde{\mathbf{a}}$ will be used for reduced domain quantities. Furthermore, a *coupling boundary* will be defined to couple the domains together, the shape of which is defined by *coupling nodes*. In the general case, this coupling boundary does not need to conform exactly to the boundaries of either the main or reduced domains.

A slightly similar domain decomposition approach with Dirichlet-to-Neumann mapping (DtN) was presented in [25]. This DtN method was based on a regular tessellation of a winding, with one hexagonal tile per conductor. However, this approach would be difficult to apply to more complex slot shapes with a non-uniform packing of conductors. Thus, in this paper the entire slot is modelled at once. The computation cost for the reduced domain is of course higher, but should not be intolerable with typical slot shapes and realistic mesh densities. Additionally, using the DtN method on the uneven packing would probably require solving several reduced domain problems with different tile shapes, increasing both the solution and overhead times.

Furthermore, the DtN method required a conforming meshing at the boundary between main and reduced domains. By contrast, the proposed method allows for discrepancies between the meshes and even the geometries themselves. Finally, the DtN method had a minimum of 2 DoFs per conductor in the main domain analysis, whereas the proposed method has DoFs only on the coupling boundary. Indeed, in the examples good results shall be seen with only 60 DoFs per slot, where the DtN method would have required at least 672.

A. A-V Formulation

In this paper, the well-known A-V formulation is used, so the solution of the Galerkin-discretized field-circuit problem consists of the vector potential $\mathbf{a}$, voltages $\mathbf{u}$ over the conductors and a set of linearly independent currents (typically loop currents) $\mathbf{i}$ [26]. Thus the problem can be expressed as

$$\begin{bmatrix} \mathbf{S}+\mathbf{M}\frac{\mathrm{d}}{\mathrm{d}t} & \mathbf{C}_\mathrm{J} & \mathbf{0} \\ \mathbf{C}_\mathrm{E}\frac{\mathrm{d}}{\mathrm{d}t} & -\mathbf{I} & \mathbf{R}\mathbf{L} \\ \mathbf{0} & \mathbf{L}^\mathrm{T} & \mathbf{Z} \end{bmatrix} \begin{bmatrix} \mathbf{a} \\ \mathbf{u} \\ \mathbf{i} \end{bmatrix} = \begin{bmatrix} \mathbf{0} \\ \mathbf{0} \\ \mathbf{u}_\mathrm{s} \end{bmatrix}, \tag{1}$$

where $\mathbf{S}$ and $\mathbf{M}$ are the well-known stiffness and mass matrices respectively. The matrices $\mathbf{C}_\mathrm{J}$ and $\mathbf{C}_\mathrm{E}$ with the entries

$$[\mathbf{C}_\mathrm{J}]_{ij} = \frac{-\sigma}{l_\mathrm{e}} \int_{\Omega_j^\mathrm{c}} \varphi_i \mathrm{d}S \tag{2}$$

$$[\mathbf{C}_\mathrm{E}]_{ij} = R_i \int_{\Omega_i^\mathrm{c}} \varphi_j \mathrm{d}S \tag{3}$$

describe the current density in the conductors due to the voltages $\mathbf{u}$, and the back-emfs induced on the conductors, respectively. The shape function of the node i is denoted by φ_i. The conductivity and axial length are denoted by σ and l_e, whereas Ω and Ω_i^c are the entire problem domain, and the domain of the conductor i respectively. Finally, $\mathbf{R}$ is a diagonal matrix of the conductor resistances R_i, $\mathbf{Z}$ is the end-winding impedance, and $\mathbf{L}$ is the loop matrix describing the winding connection, with the entries

$$[\mathbf{L}]_{ij} = \begin{cases} 1 & \text{current } j \text{ flows through conductor } i \text{ forwards} \\ -1 & \text{current } j \text{ flows through conductor } i \text{ backwards} \\ 0 & \text{otherwise.} \end{cases} \tag{4}$$

B. Solution on the Reduced Domain

Now, only a single slot of the machine is considered, on the domain Ω^s with N_c conductors. Time-harmonic analysis is considered first, so the time-derivatives are replaced with $\mathrm{j}\omega$. The notation $\mathbf{Q} = \mathbf{S} + \mathrm{j}\omega\mathbf{M}$ is adopted for brevity. Within the slot, the reduced-domain $\tilde{\mathbf{a}}$ and $\tilde{\mathbf{u}}$ are fully determined by the currents $\tilde{\mathbf{i}}$ flowing in the conductors, and the boundary values of the vector potential on the boundary $\partial\Omega^\mathrm{s}$. For generality, all conductors are assumed to be parallel-connected, so $\tilde{\mathbf{u}}$ and $\tilde{\mathbf{i}}$ have the same size. Due to the absence of iron components, the problem can be assumed linear.

Indeed, the solution of this discrete problem is spanned by a finite number of boundary data. Firstly, let $n_1, n_2, \ldots, n_{N^\mathrm{bnd}}$ be the boundary nodes of some meshing for Ω^s, and $\partial\tilde{\mathbf{a}}$ denote the nodal potentials on the boundary. Next, a set of solutions is computed

$$\mathbf{X}^\mathrm{A} = \begin{bmatrix} \mathbf{x}_1^\mathrm{A} & \mathbf{x}_2^\mathrm{A} & \ldots & \mathbf{x}_{N^\mathrm{bnd}}^\mathrm{A} \end{bmatrix}, \tag{5}$$

with each solution

$$\mathbf{x}_k^\mathrm{A} = \begin{bmatrix} \tilde{\mathbf{a}}_k^\mathrm{A} \\ \tilde{\mathbf{u}}_k^\mathrm{A} \end{bmatrix} \tag{6}$$

corresponding to the following boundary data

$$\partial\tilde{\mathbf{a}}_k = \begin{cases} 1 & \text{at } n_k \\ 0 & \text{elsewhere} \end{cases}$$
$$\tilde{\mathbf{i}} = \mathbf{0}. \tag{7}$$

Likewise, another set of solutions is computed

$$\mathbf{X}^\mathrm{I} = \begin{bmatrix} \mathbf{x}_1^\mathrm{I} & \mathbf{x}_2^\mathrm{I} & \ldots & \mathbf{x}_{N_\mathrm{c}}^\mathrm{I} \end{bmatrix} \tag{8}$$

for the unit current sources

$$\partial\tilde{\mathbf{a}} = \mathbf{0}$$
$$\left[\tilde{\mathbf{i}}_k\right]_i = \begin{cases} 1 & i = k \\ 0 & i \neq k. \end{cases} \tag{9}$$

Both $\mathbf{X}^\mathrm{A}$ and $\mathbf{X}^\mathrm{I}$ can be easily obtained based on (1) by solving problems of type

$$\begin{bmatrix} \tilde{\mathbf{Q}} & \tilde{\mathbf{C}}_\mathrm{J} \\ \mathrm{j}\omega\tilde{\mathbf{C}}_\mathrm{E} & -\mathbf{I} \end{bmatrix} \mathbf{x} = \begin{bmatrix} -\mathbf{Q}_\mathrm{bnd}\partial\mathbf{a} \\ -\tilde{\mathbf{R}}\mathbf{i} \end{bmatrix}, \tag{10}$$

where $\mathbf{Q}_{\mathrm{bnd}}$ is the stiffness-mass matrix related to the non-zero Dirichlet boundary condition.

Now, the discretized solution on Ω^{s} for any arbitrary combination of currents $\tilde{\mathbf{i}}$ and boundary potential $\partial\tilde{\mathbf{a}}$ can be expressed as a linear combination of $\mathbf{X}^{\mathrm{A}}$ and $\mathbf{X}^{\mathrm{I}}$ as

$$\begin{bmatrix}\tilde{\mathbf{a}}\\ \tilde{\mathbf{u}}\end{bmatrix} = \begin{bmatrix}\mathbf{X}^{\mathrm{A}} & \mathbf{X}^{\mathrm{I}}\end{bmatrix}\begin{bmatrix}\partial\tilde{\mathbf{a}}\\ \tilde{\mathbf{i}}\end{bmatrix}. \tag{11}$$

Indeed, this solution is exactly the same (within numerical accuracy) as would be obtained by explicitly solving (10) with the same boundary data.

C. Extension to Time-Domain

To extend the method to the time-domain, impulse response functions and convolutions can be utilized, as suggested in [25] and utilized for a different formulation in [27]. For simplicity, a constant time-step length is assumed. With this assumption, it is sufficient to replace $\mathbf{X}^{\mathrm{A}}$ and $\mathbf{X}^{\mathrm{I}}$ by the corresponding discrete-time impulse response functions $\mathbf{H}^{\mathrm{A}}[n]$ and $\mathbf{H}^{\mathrm{I}}[n]$. The bracket notation $[n]$ is used to denote the dependence on the number of time-step n.

Both are matrix-valued functions, with e.g. the k^{th} column of $\mathbf{H}^{\mathrm{A}}$ consisting of the solution $\tilde{\mathbf{a}}^{\mathrm{A}}[n]$ and $\tilde{\mathbf{u}}^{\mathrm{A}}[n]$ corresponding to the boundary data

$$\begin{aligned}\partial\tilde{\mathbf{a}}_k[n] &= \begin{cases}\delta[n] & \text{at } n_k\\ 0 & \text{elsewhere}\end{cases}\\ \tilde{\mathbf{i}} &= \mathbf{0}.\end{aligned} \tag{12}$$

Here, δ is the discrete-time impulse function

$$\delta[n] = \begin{cases}1 & n = 1\\ 0 & \text{otherwise.}\end{cases} \tag{13}$$

$\mathbf{H}^{\mathrm{I}}$ is defined analogously to (8). Both can be determined with time-stepping analysis, starting from all-zero conditions at $n = 0$.

Then, the solution with arbitrarily-varying excitation can be obtained with the discrete convolution

$$\begin{aligned}\begin{bmatrix}\tilde{\mathbf{a}}\\ \tilde{\mathbf{u}}\end{bmatrix}[n] &= \mathbf{H}^{\mathrm{A}}[1]\partial\tilde{\mathbf{a}}[n] + \mathbf{H}^{\mathrm{I}}[1]\tilde{\mathbf{i}}[n]\\ &\quad + \sum_{l=1}^{n-1}\mathbf{H}^{\mathrm{A}}[n-l+1]\partial\tilde{\mathbf{a}}[l] + \mathbf{H}^{\mathrm{I}}[n-l+1]\tilde{\mathbf{i}}[l],\end{aligned} \tag{14}$$

where the values corresponding to the newest time-step have been intentionally separated on the first row. Also this solution will be exact, as the slot is a linear time-invariant (LTI) system and hence fully characterized by its impulse response function. The above is valid for zero initial conditions, but non-zero ones can be considered by including an additional zero-input decay term [27].

D. Boundary Interpolation

Due to meshing requirements, the number of boundary nodes N^{bnd} will often be much larger than would be necessary to reasonably approximate any realistic boundary values $\partial\mathbf{a}$. Therefore, obtaining $\mathbf{X}^{\mathrm{A}}$ would present a large, mostly unnecessary computational burden. Thus, the isoparametric FE approach of order p is utilized here.

The coupling boundary C approximating $\partial\Omega^{\mathrm{s}}$ is defined as follows. A total $N^{\mathrm{cpl}} < N^{\mathrm{bnd}}$ coupling nodes located at $\hat{\mathbf{x}}_1, \ldots, \hat{\mathbf{x}}_{N^{\mathrm{cpl}}}$ are defined, with the $\hat{\mathbf{x}}$ falling on or near $\partial\Omega^{\mathrm{s}}$. A set of N^{cpl}/p (possibly curved) edges is defined to connect these nodes, with $p+1$ points on each edge and each end-point shared with the adjacent edge. Next, a 1D reference edge is defined with $p+1$ nodes $\hat{t}_i$ equally distributed on $[0,1]$, so that it is easy to define a set of polynomial shape functions $\hat{\psi}$ satisfying

$$\hat{\psi}_k(t) = \begin{cases}1 & t = \hat{t}_k\\ 0 & t = \hat{t}_i, \quad i \neq k.\end{cases} \tag{15}$$

Then, each global edge e is defined by

$$\mathbf{x} = \sum_{k=1}^{p+1}\hat{\mathbf{x}}_{n_k^e}\hat{\psi}_k(t), \quad t \in [0,1], \tag{16}$$

where $\hat{\mathbf{x}}_{n_k^e}$ are the $p+1$ nodes belonging the edge. The final approximation C of $\partial\Omega^{\mathrm{s}}$ is then the union of these edges.

The boundary values $\partial\tilde{\mathbf{a}}$ can then be defined as a linear combination of a new set of N^{cpl} independent vector potential values $\partial\hat{\mathbf{a}}$ as follows. For each boundary node n_i of the meshing for Ω^{s}, the closest point on C is determined. If this point falls on the edge e with the corresponding reference coordinate t_i, the boundary potential is set to

$$[\partial\tilde{\mathbf{a}}]_i = \sum_{k=1}^{p+1}[\partial\hat{\mathbf{a}}]_{n_k^e}\,\hat{\psi}_k(t_i). \tag{17}$$

In practice, the closest point on C can be easily obtained by minimizing the distance with a few iterations of the Newton's method. The initial guess can be explicitly obtained by using a linear approximation of each edge with their end nodes only, and finding the closest point on that line segment.

The constant coefficients $\hat{\psi}_k(t_i)$ are then collected to a matrix $\mathbf{P}_{\mathrm{cr}}$, so that the relationship between $\partial\tilde{\mathbf{a}}$ and $\partial\hat{\mathbf{a}}$ can be compactly expressed as

$$\partial\tilde{\mathbf{a}} = \mathbf{P}_{\mathrm{cr}}\partial\hat{\mathbf{a}}. \tag{18}$$

Now, it is sufficient to compute $\mathbf{X}^{\mathrm{A}}$ for different $\partial\hat{\mathbf{a}}$ only.

The approach is illustrated in Fig. 1(a), in which a second-order edge (blue) is used to approximate a quarter-circle slot bottom half (black). The end-nodes of the edge are plotted with the circles, while a dot is used for the center node. As can be seen, even this coarse approximation matches the boundary shape relatively well. The shape function values associated with the center node (red) and end node (blue) of the edge are also shown in Fig 1(b).

E. Coupling to the Main Domain

Now, the remaining task is to utilize the slot solutions for obtaining the solution for entire domain Ω in an efficient fashion. The case with only one slot is considered for clarity,

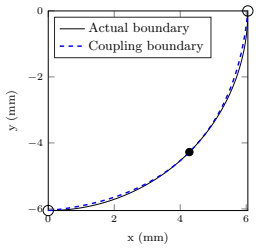

(a) A circular boundary approximated with a second-order coupling boundary.

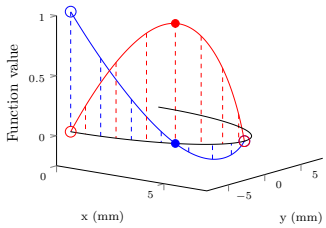

(b) Boundary shape functions.

Fig. 1. Illustration of the isoparametric coupling boundary.

assuming only the reduced domain has conducting parts. The harmonic discrete problem can then be written as

$$\begin{aligned} \mathbf{S}\mathbf{a} &= 0 \\ \tilde{\mathbf{Q}}\tilde{\mathbf{a}} + \tilde{\mathbf{C}}_{\mathrm{J}}\tilde{\mathbf{u}} &= 0 \\ \mathbf{L}^{\mathrm{T}}\tilde{\mathbf{u}} + \mathbf{Z}\tilde{\mathbf{i}} &= \mathbf{u}_{\mathrm{s}}, \end{aligned} \tag{19}$$

where the first equation governs the main domain. By writing $\mathbf{a}_{\mathrm{r}}$ and $\mathbf{u}_{\mathrm{r}}$ with (11) and redefining the test-function side as $\mathbf{a}^{\mathrm{A}}$, the latter two equations can be re-written as

$$\begin{aligned} \hat{\mathbf{R}}_{\mathrm{AA}}\partial\hat{\mathbf{a}} + \hat{\mathbf{R}}_{\mathrm{AI}}\mathbf{L}\tilde{\mathbf{i}} &= 0 \\ \mathbf{L}^{\mathrm{T}}\hat{\mathbf{R}}_{\mathrm{UA}}\partial\hat{\mathbf{a}} + \mathbf{L}^{\mathrm{T}}\hat{\mathbf{R}}_{\mathrm{UI}}\mathbf{L}\tilde{\mathbf{i}} + \mathbf{Z}\tilde{\mathbf{i}} &= \mathbf{u}_{\mathrm{s}} \end{aligned} \tag{20}$$

with the newly-introduced reduced matrices

$$\hat{\mathbf{R}}_{\mathrm{AA}} = (\tilde{\mathbf{a}}^{\mathrm{A}})^{\mathrm{T}}\tilde{\mathbf{Q}}\tilde{\mathbf{a}}^{\mathrm{A}} + (\tilde{\mathbf{a}}^{\mathrm{A}})^{\mathrm{T}}\tilde{\mathbf{C}}_{\mathrm{J}}\tilde{\mathbf{u}}^{\mathrm{A}} \tag{21}$$

$$\hat{\mathbf{R}}_{\mathrm{AI}} = (\tilde{\mathbf{a}}^{\mathrm{A}})^{\mathrm{T}}\tilde{\mathbf{Q}}\tilde{\mathbf{a}}^{\mathrm{I}} + (\tilde{\mathbf{a}}^{\mathrm{A}})^{\mathrm{T}}\tilde{\mathbf{C}}_{\mathrm{J}}\tilde{\mathbf{u}}^{\mathrm{I}} \tag{22}$$

$$\hat{\mathbf{R}}_{\mathrm{UA}} = \tilde{\mathbf{u}}^{\mathrm{A}} \tag{23}$$

$$\hat{\mathbf{R}}_{\mathrm{UI}} = \tilde{\mathbf{u}}^{\mathrm{I}}. \tag{24}$$

Indeed, the solution of the main problem only consists of $\mathbf{a}$ for representing the main domain solution, and $\partial\hat{\mathbf{a}}$ and $\tilde{\mathbf{i}}$ for representing the reduced domain solution. Furthermore, since the slot is magnetically linear, and all the nonlinear parts are modelled by standard means, extension to nonlinear problems is straightforward.

Time-domain is handled in a similar fashion, only (14) is used instead of (11). $\mathbf{H}^{\mathrm{A}}[1]$ and $\mathbf{H}^{\mathrm{I}}[1]$ are used to form the reduced matrices, while the remaining convolution terms contribute to the load vector only. The previous time-step values of $\tilde{\mathbf{a}}$ are also considered on the right-hand side, depending on the particular time-stepping scheme used.

Finally, the main and reduced domains have to be coupled together at the slot boundary. In this paper, $\partial\hat{\mathbf{a}}$ are retained as independent variables, and the boundary potentials of the main domain are interpolated as $\partial\mathbf{a} = \mathbf{P}_{\mathrm{cm}}\partial\hat{\mathbf{a}}$ and eliminated. The interpolation matrix $\mathbf{P}_{\mathrm{cm}}$ can be obtained with the same procedure as described in (15)-(18).

Obviously, the coupling nodes could also be slaved to the main domain instead of vice versa. However, it is a common practice to use the higher-reluctivity side of the boundary as the master variable, in e.g. the mortar element method. Furthermore, in the computation examples it shall be seen that using a larger number of coupling nodes can improve accuracy even with a coarse main mesh.

This approach allows for a great freedom in representing the main domain. Curved boundaries can be approximated very coarsely if desired, i.e. the geometry itself can be nonconforming with both the reduced domain and the coupling boundary. Even with a fully conforming geometry, the main mesh nodes do not have to coincide with the coupling nodes. This is a great benefit with many meshing tools, in which specifying boundary nodes is difficult. Furthermore, the density of coupling nodes can be adjusted freely based on the assumed smoothness of the solution on the boundary.

F. Precision of the Proposed Method

It must be noted that the proposed method is theoretically exact under suitable conditions. Specifically, consider a 2D machine geometry meshed in a normal fashion. Naturally, each slot-mesh can be extracted as a reduced domain, modelled as described in this paper, and then coupled back to the rest of the domain. With exact arithmetic, this solution will be equal to that obtained by solving the original problem by non-reduced FEM, using the same mesh. In reality, the limited floating-point precision will of course introduce some error, but these deviations should be minor. Indeed, this particular case shall be demonstrated in Section III-B.

III. Simulations

This section is divided into two parts. The first one focuses on the coupling boundary, evaluating how the number of coupling nodes and the order of the interpolation influences the accuracy of the method. To eliminate confounding factors, a simplified linear problem is analysed in the frequency domain. By contrast, the latter part demonstrates the performance of the method on a realistic problem. A 500 kW induction motor at rated load is analysed, utilizing nonlinear analysis both in the frequency- and time-domains.

A. Single Slot Segment

The performance of the proposed method was first evaluated on a slot segment of a simplified high-speed induction machine. The main dimensions of the machine can be found in Table I. Two slot shapes were analysed, shown in Fig. 2. The rotor of the machine was ignored, since analysing a solid conducting rotor would have been challenging in itself and could thus have confounded the results.

The methods were compared to a reference solution, obtained by densely meshing the entire problem domain. Thus, part of the observed error can be explained by the discretization error, i.e. limitations imposed by the coarser mesh used. Section III-B will later analyse a problem with identical meshes in both solutions, cancelling this error component.

TABLE I
MAIN DIMENSIONS OF THE HIGH-SPEED MACHINE.

Winding connection	Delta
Number of parallel paths	2
Number of winding layers	2
Number of turns	3
Number of strands per slot	336
Number of stator slots	36
Coil pitch (slots)	12
Stator diameter (mm)	288

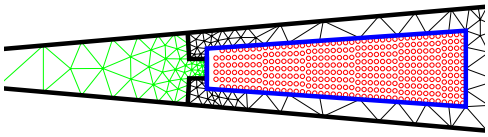

(a)

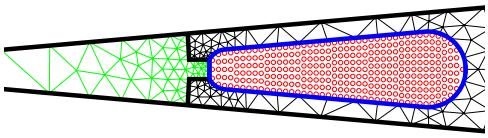

(b)

Fig. 2. The two slot shapes analysed. The coarsest main mesh is also shown. Air domain is plotted in green, whereas the reduced domain is highlighted in blue.

1) Trapezoidal Slot: The trapezoidal slot shape of Fig. 2(a) was analysed first. The supply frequency was set to 6050 Hz, corresponding to the 11th harmonic of the fundamental often present in pulse-amplitude modulation. The winding connection was set to correspond to the first slot of the machine, i.e. with phases (a) and -(c).

The reduced domain was meshed with two layers of elements per strand, resulting in 21789 nodal DoFs. For a reference solution, a brute-force simulation was performed with the entire segment densely meshed with 153405 DoFs. A part of the reduced domain mesh near the slot bottom corner has been illustrated in Fig. 3.

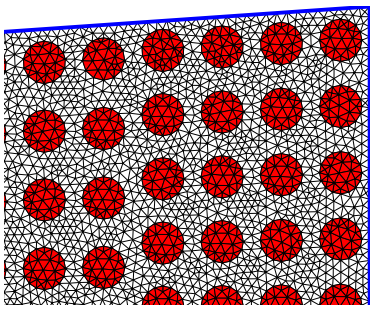

Fig. 3. A part of the reduced domain mesh. Strands have been highlighted in red.

The fully conforming case was analysed first, i.e. with the coupling nodes coinciding with the main mesh nodes as shown in Fig. 4. The initial coarse discretization shown in Figure 2(a) resulted in 141 nodes in the mesh, of which 30 were coupling nodes. The iron part of the mesh was later uniformly refined and the simulations were repeated.

The results are shown in Table II. Shown are the number of coupling nodes, and the relative errors $||\mathbf{i} - \mathbf{i}_{\text{ref}}||/||\mathbf{i}_{\text{ref}}||$, $||\mathbf{P} - \mathbf{P}_{\text{ref}}||/||\mathbf{P}_{\text{ref}}||$ between the vectors of currents and the per-conductor total losses. Unsurprisingly, refining the mesh improved accuracy.

The simulations were repeated for a non-conforming case, with the coupling nodes defined independently from either mesh and spaced approximately uniformly on the boundary. An example is again illustrated in Fig. 5. Both first- and second-order coupling boundaries were analysed, and the results are shown in Table III. It can be seen that with 30 nodes, the errors were roughly 50% smaller than in the conforming case with 37. This can be probably mainly be attributed to the distribution of coupling nodes: the nonconforming approach had a larger portion of the coupling on the slot sides where $\mathbf{a}$ exhibited sharp spatial changes due to the circulating currents. However, the order of boundary did not have any consistent effect on accuracy.

TABLE II
RESULTS WITH THE COUPLING NODES CORRESPONDING TO THE MAIN MESH NODES (TRAPEZOIDAL SLOT)

No. of coupling nodes	$\mathbf{i}$ error (%)	$\mathbf{P}$ error (%)
37	11.50	9.11
74	5.94	5.41
296	0.54	0.28

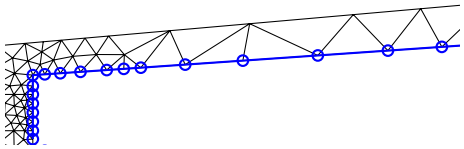

Fig. 4. A part of the coupling boundary illustrated. The coupling nodes correspond to the main mesh nodes.

TABLE III
RESULTS WITH THE COUPLING NODES INDEPENDENTLY DISTRIBUTED ON THE BOUNDARY (TRAPEZOIDAL SLOT)

No. of coupling nodes	Bnd. Order	$\mathbf{i}$ error (%)	$\mathbf{P}$ error (%)
33	1	6.31	5.58
62	1	1.17	0.87
62	2	1.10	0.85
112	1	0.632	0.352
112	2	0.648	0.362

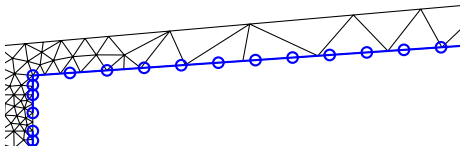

Fig. 5. A part of the coupling boundary illustrated. The coupling nodes are independently distributed.

2) Rounded Slot: The rounded slot of Fig. 2(b) was analysed next. The frequency was also increased to 50 kHz,

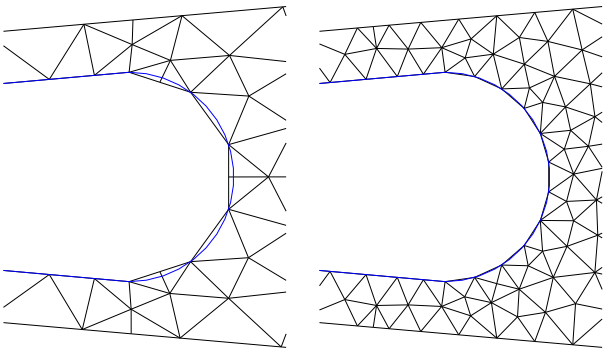

(a) (b)

Fig. 6. Main meshes of two different refinement levels. The boundary of the reduced domain has been highlighted in blue.

often used as switching frequency in pulse-width modulation. In the previous example, the domain boundaries consisted of a few linear segments. Thus, the actual geometries of the main and reduced domain conformed to each other at the boundary, even though the coupling nodes and the main mesh nodes did not. As can be seen from the close-ups in Fig. 6, this was no longer the case. Furthermore, refining the main mesh had a direct effect on this level of nonconformity, visible in the right subfigure.

Two types of approaches were again evaluated. Table IV shows the results with coupling boundary conforming to the main domain, and the coupling nodes matching the main mesh nodes. By contrast, in Table V the coupling boundary conformed approximately to the reduced domain, and the coupling nodes were spaced approximately equally on the boundary. In the latter case, only the coarsest main mesh was utilized.

Once again, the latter approach fared better. Furthermore, in this case using a second-order boundary seemed to yield a small but consistent improvement in accuracy. This is most likely explained by the ability of the nonlinear boundary to better approximate the curved geometry with a smaller number of coupling nodes. Indeed, the last two simulations with the highest number of nodes were approximately on par.

TABLE IV
RESULTS WITH THE COUPLING NODES CORRESPONDING TO THE MAIN MESH NODES (ROUNDED SLOT)

No. of coupling nodes	$\mathbf{i}$ error (%)	$\mathbf{P}$ error (%)
41	13.19	10.62
75	5.49	4.58
116	4.44	4.61

B. 500 kW Induction Machine

To evaluate the method on a realistic problem, a 500 kW random-wound induction motor was analysed. Nonlinear analysis was performed both in the frequency and time-domains at the rated load. The main dimensions are listed in Table VI. As can be seen, the machine had 112 conductors in one slot, corresponding to 5376 in the entire symmetry sector of 48 stator slots. Each turn consisted of 28 parallel strands. Each turn was further divided into 4 bundles, the order of which was transposed 180 degrees between slots to limit the circulating current losses.

TABLE V
RESULTS WITH THE COUPLING NODES INDEPENDENTLY DISTRIBUTED ON THE BOUNDARY (ROUNDED SLOT)

No. of coupling nodes	Bnd. Order	$\mathbf{i}$ error (%)	$\mathbf{P}$ error (%)
38	1	10.49	9.46
38	2	9.84	8.73
60	1	3.83	3.52
60	2	3.57	2.98
94	1	1.72	1.79
94	2	1.74	1.48

The main and reduced domains were meshed with 4766 and 7589 elements, respectively, and the coupling nodes were chosen to correspond to the main mesh boundary nodes. The reference solution was computed utilizing the same meshes, enforcing the continuity of the potential with the interpolation method recently shown to perform well in electromagnetic problems [28].

TABLE VI
MAIN DIMENSIONS OF THE INDUCTION MACHINE.

Rated frequency (Hz)	50
Slip (%)	0.637
Winding connection	Delta
Number of winding layers	2
Number of strands per slot	112
Number of turns	2
Number of stator slots	96
Number of rotor slots	74
Stator diameter (mm)	600
Length (mm)	760

In time-harmonic analysis, both the proposed method and the reference solution took 17 Newton iterations to converge. As can be seen from the breakdown of computational costs in Table VII, the proposed method was roughly 90 times faster. The relative error in the loop currents was 9.75×10^{-14}, and the relative L2-norm error in the vector potential 4.64×10^{-12}. As can be seen, the proposed method now indeed yielded a precision almost on par with the computation precision. This result conforms to the theory, as both solutions utilized the same mesh which excluded the discretization error from the comparison.

TABLE VII
COMPUTATIONAL COSTS IN HARMONIC ANALYSIS.

	Proposed Method	**Reference**
Total computation time	3.67 s	5 min 30 s
• Pre-computation	0.65 s	-
• Jacobian factorization	2.04 s	4 min 13 s

Next, time-stepping analysis was performed using a PWM voltage supply. The voltage waveforms were generated with the sine-triangle comparison scheme with a switching

frequency of 2.5 kHz and a modulation index of $\pi/4$. A single period of the supply period was analysed, with a total of 1200 time-steps of equal lengths.

A comparison of the computational costs can again be found in Table VIII. This time, the proposed approach was approximately 54 times faster, with a significant a mount of time spent on computing the discrete convolutions. Fig. 7 then shows the two error norms as functions of time. Both stayed well below 10^{-10} during the entire simulation.

TABLE VIII
COMPUTATIONAL COSTS IN TIME-STEPPING ANALYSIS.

	Proposed Method	**Reference**
Total computation time	7 min 21 s	6 h 34 min
• Pre-computation	5.61 s	-
• Convolution	3 min 16 s	-
• Jacobian factorization	2 min 31 s	4 h 42 min

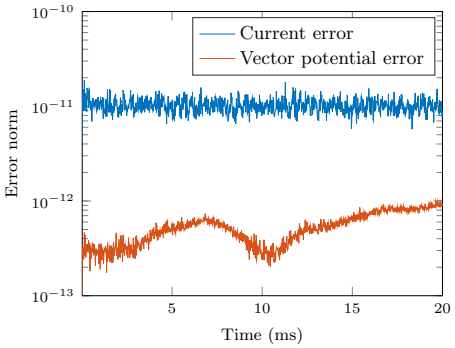

Fig. 7. Relative error norms of the loop currents and vector potential as functions of time.

Fig. 8 then shows the contribution of the AC phenomena to the stator resistive losses. These are expressed as a relative increase from ideal losses, which were computed by from the phase currents and phase DC resistances. The circulating current losses were computed from the loop currents and the DC resistances of the conductors, and the remaining losses were attributed to the skin- and proximity effects. On average, their contributions were 6.7 and 22 % respectively. However, both exhibited large peaks immediately after the supply voltage switches as evident in Fig. 8.

Finally, Fig. 9 shows the current density distribution in slot 1 at $t \approx 18$ ms, immediately after a voltage switch. Clearly, the distribution differs from the typical skin effect pattern, where the current crowds towards the slot opening. This deviation can be attributed to the circulating currents, as the conductors in the slot are now carrying different currents.

IV. CONCLUSIONS AND DISCUSSION

A method was proposed for efficient finite element computation of resistive losses in the windings of electrical machines. The field-circuit problem was first solved in a single slot with different boundary conditions. These solutions were then used as basis functions in all slots of the machine, and

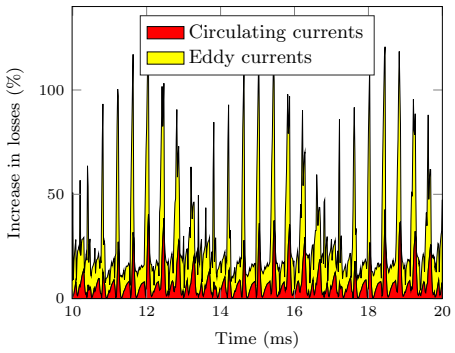

Fig. 8. Contributions of different resistive loss components, as a relative increase from losses computed with the DC approximation.

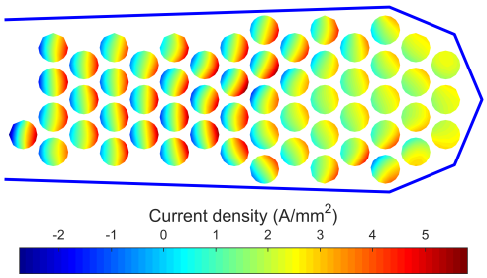

Fig. 9. Current density in the bottom layer of slot 1 at $t \approx 18$ ms.

coupled together with the traditional nodal shape functions on the boundary. For this coupling, an isoparametric approach was proposed, allowing for easy handling of nonconformity on the mesh or even geometry level.

The proposed coupling method was first evaluated on a simplified linear time-harmonic problem. According to the simulations, it appears to handle curved boundaries and inter-domain nonconformity in a robust fashion. Particularly, the coupling nodes can be determined independently from either of the two meshes used. If the main mesh is coarse, this practice may improve accuracy. Next, a 500 kW induction motor was analysed in both frequency- and time-domains to evaluate the method on a realistic nonlinear problem. In both cases, the method yielded very precise results, 90 and 54 times faster compared to the reference solution, respectively.

It must be noted that the proposed method has not been verified experimentally, so the results must be regarded with certain reservations. However, the method *was* shown to precisely match the results of the well-established 2D finite element analysis. Furthermore, 2D-FEM is already generally accepted as a valid design tool, and its accuracy has indeed been experimentally demonstrated also for multi-conductor windings like the ones analysed in this paper, in e.g. [15], [18], [22], [23]. Thus, the proposed method could be regarded as a time-saving modification to it. As such, it could be suitable for the design and analysis of high-performance electrical machines, where a large number of design candidates may have to be analysed fast.

REFERENCES

[1] J. Gyselinck and P. Dular, "Frequency-domain homogenization of bundles of wires in 2-D magnetodynamic FE calculations," *IEEE Trans. Magn.*, vol. 41, no. 5, pp. 1416–1419, May 2005.

[2] J. Gyselinck, P. Dular, N. Sadowski, P. Kuo-Peng, and R. Sabariego, "Homogenization of form-wound windings in frequency and time domain finite-element modeling of electrical machines," *IEEE Trans. Magn.*, vol. 46, no. 8, pp. 2852–2855, Aug 2010.

[3] R. Sabariego, P. Dular, and J. Gyselinck, "Time-domain homogenization of windings in 3-D finite element models," *IEEE Trans. Magn.*, vol. 44, no. 6, pp. 1302–1305, June 2008.

[4] J. Gyselinck, R. Sabariego, and P. Dular, "Time-domain homogenization of windings in 2-D finite element models," *IEEE Trans. Magn.*, vol. 43, no. 4, pp. 1297–1300, April 2007.

[5] Z. De Greve, O. Deblecker, J. Lobry, and J.-P. Keradec, "High-frequency multi-winding magnetic components: From numerical simulation to equivalent circuits with frequency-independent RL parameters," *IEEE Trans. Magn.*, vol. 50, no. 2, pp. 141–144, Feb 2014.

[6] J. Sibue, J. Ferrieux, G. Meunier, and R. Periot, "Modeling of losses and current density distribution in conductors of a large air-gap transformer using homogenization and 3-D FEM," *IEEE Trans. Magn.*, vol. 48, no. 2, pp. 763–766, Feb 2012.

[7] J.-R. Sibue, G. Meunier, J.-P. Ferrieux, J. Roudet, and R. Periot, "Modeling and computation of losses in conductors and magnetic cores of a large air gap transformer dedicated to contactless energy transfer," *IEEE Trans. Magn.*, vol. 49, no. 1, pp. 586–590, Jan 2013.

[8] X. Nan and C. Sullivan, "An equivalent complex permeability model for Litz-wire windings," *IEEE Trans. Ind. Appl.*, vol. 45, no. 2, pp. 854–860, March 2009.

[9] A. Lehikoinen, N. Chiodetto, E. Lantto, A. Arkkio, and A. Belahcen, "Monte Carlo analysis of circulating currents in random-wound electrical machines," *IEEE Trans. Magn.*, 2016, in press.

[10] A. Lehikoinen and A. Arkkio, "Efficient finite-element computation of circulating currents in thin parallel strands," *IEEE Trans. Magn.*, vol. 52, no. 3, pp. 1–4, March 2016.

[11] M. van der Geest, H. Polinder, J. Ferreira, and D. Zeilstra, "Current sharing analysis of parallel strands in low-voltage high-speed machines," *IEEE Trans. Ind. Electron.*, vol. 61, no. 6, pp. 3064–3070, June 2014.

[12] F. Jiancheng, L. Xiquan, B. Han, and K. Wang, "Analysis of circulating current loss for high-speed permanent magnet motor," *IEEE Trans. Magn.*, vol. 51, no. 1, pp. 1–13, Jan 2015.

[13] J. D. Widmer, R. Martin, and B. C. Mecrow, "Precompressed and stranded aluminum motor windings for traction motors," *IEEE Trans. Ind. Appl.*, vol. 52, no. 3, pp. 2215–2223, May 2016.

[14] V. Sung and W. G. Odendaal, "Litz wire pulsed power air core coupled inductor," *IEEE Trans. Ind. Appl.*, vol. 51, no. 4, pp. 3385–3393, July 2015.

[15] R. Wrobel, D. Staton, R. Lock, J. Booker, and D. Drury, "Winding design for minimum power loss and low-cost manufacture in application to fixed-speed PM generator," *IEEE Trans. Ind. Appl.*, vol. 51, no. 5, pp. 3773–3782, Sept 2015.

[16] M. Fujita, Y. Kabata, T. Tokumasu, K. Nagakura, M. Kakiuchi, and S. Nagano, "Circulating currents in stator coils of large turbine generators and loss reduction," *IEEE Trans. Ind. Appl.*, vol. 45, no. 2, pp. 685–693, March 2009.

[17] M. Islam, S. Mir, and T. Sebastian, "Effect of paralleling the stator coils in a permanent-magnet machine," *IEEE Trans. Ind. Appl.*, vol. 42, no. 6, pp. 1429–1436, Nov 2006.

[18] M. Vetuschi and F. Cupertino, "Minimization of proximity losses in electrical machines with tooth-wound coils," *IEEE Trans. Ind. Appl.*, vol. 51, no. 4, pp. 3068–3076, July 2015.

[21] L. J. Wu, Z. Q. Zhu, D. Staton, M. Popescu, and D. Hawkins, "Analytical model of eddy current loss in windings of permanent-

[19] A. Tessarolo, F. Agnolet, F. Luise, and M. Mezzarobba, "Use of time-harmonic finite-element analysis to compute stator winding eddy-current losses due to rotor motion in surface permanent-magnet machines," *IEEE Trans. Energy Convers.*, vol. 27, no. 3, pp. 670–679, Sept 2012.

[20] Y. Amara, P. Reghem, and G. Barakat, "Analytical prediction of eddy-current loss in armature windings of permanent magnet brushless AC machines," *IEEE Trans. Magn.*, vol. 46, no. 8, pp. 3481–3484, Aug 2010.

magnet machines accounting for load," *IEEE Trans. Magn.*, vol. 48, no. 7, pp. 2138–2151, July 2012.

[22] S. Iwasaki, R. P. Deodhar, Y. Liu, A. Pride, Z. Q. Zhu, and J. J. Bremner, "Influence of PWM on the proximity loss in permanent-magnet brushless AC machines," *IEEE Trans. Ind. Appl.*, vol. 45, no. 4, pp. 1359–1367, July 2009.

[23] A. G. Sarigiannidis and A. G. Kladas, "Switching frequency impact on permanent magnet motors drive system for electric actuation applications," *IEEE Trans. Magn.*, vol. 51, no. 3, pp. 1–4, March 2015.

[24] A. Lehikoinen, A. Arkkio, and A. Belahcen, "Reduced basis finite element modelling of electrical machines with multi-conductor windings," in *22nd International Conference on Electrical Machines (ICEM)*, September 2016, pp. 1–7.

[25] L. Lehti, J. Keränen, S. Suuriniemi, and L. Kettunen, "Coil winding losses: Decomposition strategy," *IEEE Trans. Magn.*, vol. 52, no. 1, pp. 1–6, Jan 2016.

[26] I. A. Tsukerman, A. Konrad, and J. D. Lavers, "A method for circuit connections in time-dependent eddy current problems," *IEEE Trans. Magn.*, vol. 28, no. 2, pp. 1299–1302, Mar 1992.

[27] A. Lehikoinen, J. Ikäheimo, A. Arkkio, and A. Belahcen, "Domain decomposition approach for efficient time-domain finite element computation of winding losses in electrical machines," *IEEE Trans. Magn.*, pp. 1–1, 2017, (accepted for publication).

[28] G. J. Wallinger and O. Br, "3-D FE method analysis of static fields for non-conforming meshes with second-order node-based elements," *IEEE Trans. Magn.*, vol. 52, no. 3, pp. 1–4, March 2016.

V. BIOGRAPHIES

Antti Lehikoinen was born in Joensuu, Finland, in 1988. He received the B.Sc. (Tech.) and M.Sc. degrees in electromechanics from the School of Electrical Engineering, Aalto University, Espoo, Finland, in 2012 and 2013, respectively, where he is currently pursuing the Ph.D. degree.

His current research interests include stochastic modeling and prediction of additional losses due to circulating currents in random-wound machines.

Antero Arkkio was born in Vehkalahti, Finland in 1955. He received his M.Sc. (Tech.) and D.Sc. (Tech.) degrees from Helsinki University of Technology in 1980 and 1988. Currently he is a Professor of Electrical Engineering at Aalto University. His research interests deal with modeling, design, and measurement of electrical machines.

Anouar Belahcen (M13,SM15) was born in Morocco, in 1963. He received the B.Sc. degree in physics from the University Sidi Mohamed Ben Abdellah, Fes, Morocco, in 1988 and the M.Sc. (Tech.) and Doctor (Tech.) degrees from Helsinki University of Technology, Finland, in 1998, and 2004, respectively. From 2008 to 2013, he has been working as Adjunct Professor in the field of coupled problems and material modeling at Aalto University, Finland. Since 2011 he is Professor of electrical machines at Tallinn University of Technology, Estonia and in 2013 he became Professor of Energy and Power at Aalto University. His research interests are numerical modeling of electrical machines, especially magnetic material modeling, coupled magnetic and mechanical problems, magnetic forces, and magnetostriction.